HyperTime: Implicit Neural Representations for Time Series Generation

Anonymous authors
Paper under double-blind review

Abstract

Implicit neural representations (INRs) have recently emerged as a powerful tool that provides an accurate and resolution-independent encoding of data. Their robustness as general approximators has been shown in a wide variety of data sources, with applications on image, sound, and 3D scene representation. However, little attention has been given to leveraging these architectures for the representation and analysis of time series data. In this paper, we propose a new INR architecture for time series (iSIREN) designed to perform an accurate reconstruction of univariate and multivariate data, while also providing an interpretable encoding of the signal. We compare our architecture against SIREN and INRs with different activations, in terms of training convergence, and the reconstruction accuracy of both the signal and its spectral distribution. To achieve generalization, we propose a hypernetwork architecture (HyperTime) that leverages iSIRENs to learn a latent representation of an entire time series dataset. In addition to the traditional reconstruction loss, we introduce an FFT-based loss that guides the training by enforcing a good match of the ground truth spectral distribution. We show how these architectures can be used for time series generation, and evaluate our method through fidelity metrics, presenting results that exceed the performance of state-of-the-art techniques. Finally, we propose an alternative hypernetwork architecture (iHyperTime) that incorporates interpretability into the latent representation, enabling the introduction of prior knowledge by imposing constraints into the generation process.

1 Introduction

Modeling time series data has been a key topic of research for many years, constituting a crucial component in a wide variety of areas such as climate modeling, medicine, biology, retail and finance (Lim & Zohren, 2021). Traditional methods for time series modeling have relied on parametric models informed by expert knowledge. However, the development of modern machine learning methods has provided purely data-driven techniques to learn temporal relationships. In particular, neural network-based methods have gained popularity in recent times, with applications to a wide range of tasks, such as time series classification (Ismail Fawaz et al., 2020), clustering (Ma et al., 2019; Alqahtani et al., 2021), segmentation (Perslev et al., 2019; Zeng et al., 2022), anomaly detection (Choi et al., 2021; Xu et al., 2018; Hundman et al., 2018), upsampling (Oh et al., 2020; Bellos et al., 2019), imputation (Liu, 2018; Luo et al., 2018; Cao et al., 2018), forecasting (Lim & Zohren, 2021; Torres et al., 2021) and synthesis (Alaa et al., 2021; Yoon et al., 2019b; Jordon et al., 2019). In particular, generation of synthetic time series has recently gained attention due to the large number of potential applications in medical and financial fields, where data cannot be shared, either due to privacy reasons or proprietary restrictions (Jordon et al., 2021; 2019; Assefa et al., 2020). Moreover, synthetic time series can be used to augment training datasets to improve model generalization on downstream tasks, such as classification (Fons et al., 2021), forecasting and anomaly detection.

In recent years, implicit neural representations (INRs) have gained popularity as an accurate and flexible method to parameterize signals from diverse sources, such as images, video, audio and 3D scene data (Sitzmann et al., 2020b; Mildenhall et al., 2020). Conventional methods for data encoding often rely on discrete representations, such as data grids, which are limited by their spatial resolution and present inherent discretization artifacts. In contrast, INRs encode data in terms of continuous functional relationships between signals, and thus are uncoupled to spatial resolution. In practical terms, INRs provide a new data representation framework that is resolution-independent, with many potential applications to time series, where missing values and irregularly sampled data are common occurrences (Fang & Wang, 2020). While there have been a few recent works exploring the application of INRs to time series data, there is virtually no work on leveraging these architectures for generating synthetic time series or producing interpretable time series representations (Jeong & Shin, 2022; Woo et al., 2022). Applications with regulatory focus such as finance often require transparency and interpretability of proposed machine learning solutions as well as injection of expert knowledge as constraints into the training process to guide learning. For instance, explainable construction of trading agents is preferred when actions of trading agents need to be explicitly attributed to market signals (Vyetrenko & Xu, 2019).

In this paper, we propose a novel methodology that utilizes INRs to encode and generate time series data based on interpretable latent representations. To the best of our knowledge, we are the first to incorporate an interpretable decomposition into the generation of time-series. Our contributions are as follows:

Representation and Generation of time-series using INRs: We introduce iSIREN, an INR architecture for multivariate time-series representation which provides an interpretable trend-seasonality decomposition of the data. We show that interpretability does not lead to a loss of reconstruction accuracy, and in some cases increases the spectral reconstruction quality. Moreover, we leverage a hypernetwork for time-series generation via interpolation of learned embeddings.

Spectral Loss: To improve the training of the hypernetwork, we introduce a novel spectral loss that enforces the correct reconstruction of the signal's spectral distribution. We show that for some datasets this loss plays a crucial role in the learning process.

Interpretable time-series generation: We propose iHyperTime, a hypernetwork architecture for time-series generation that learns a disentangled seasonal-trend representation of time series, enabling the introduction of expert knowledge into the synthesis process. We compare iHyperTime against current state-of-the-art methods for time-series generation, showing improved results in terms of standard fidelity metrics.

2 Related Work

Implicit Neural Representations Implicit Neural Representations (INRs) provide a continuous representation of multidimensional data, by encoding a functional relationship between input coordinates and signal values, avoiding possible discretization artifacts. They have recently gained popularity in visual computing (Mescheder et al., 2019; Mildenhall et al., 2020) due to the key development of positional encodings (Tancik et al., 2020) and periodic activations (SIREN (Sitzmann et al., 2020b)), which have proven to be critical for the learning of high-frequency details. Whilst INRs have been shown to produce accurate reconstructions in a wide variety of data sources, such as video, images and audio (Sitzmann et al., 2020b; Chen et al., 2021; Rott Shaham et al., 2021), few works have leveraged them for time series representation (Jeong & Shin, 2022; Woo et al., 2022), and none have focused on interpretability and generation.

Hypernetworks Hypernetworks are neural network architectures that are trained to predict the parameters of secondary networks, referred to as Hyponetworks (Ha et al., 2017; Sitzmann et al., 2020a). In the last few years, some works have leveraged different hypernetwork architectures for the prediction of INR weights, in order to learn priors over image data (Skorokhodov et al., 2021) and 3D scene data (Littwin & Wolf, 2019; Sitzmann et al., 2019; Sztrajman et al., 2021). Sitzmann et al. (2020b) leverage a set encoder and a hypernetwork decoder to learn a prior over SIRENs encoding image data, and apply it for image in-painting. Our HyperTime and iHyperTime architectures detailed in Section 3 use a similar encoder-decoder structure, however they learn a latent representation over our interpretable SIREN INRs (iSIREN), which encode time series data. Moreover, we apply these architectures for time series generation via interpolation of learned embeddings.

Time Series Generation Synthesis of time series data using deep generative models has been previously studied in the literature. Examples include the TimeGAN architecture (Yoon et al., 2019a), as well as QuantGAN (Wiese et al., 2020). More recently, Desai et al. (2021) proposed TimeVAE as a variational autoencoder alternative to GAN-based time series generation. Alaa et al. (2021) introduced Fourier Flows, a normalizing flow model for time series data that leverages the frequency domain representation, which is currently considered together with TimeGAN as state-of-the-art for time series generation. In the last few years, multiple methods have used INRs for data generation, with applications on image synthesis (Chan et al., 2021; Skorokhodov et al., 2021), super-resolution (Chen et al., 2021) and panorama synthesis (Anokhin et al., 2021). However, there are currently no applications of INRs on the generation of time series data.

Interpretable Time Series Seasonal-trend decomposition is a standard tool in time series analysis. The trend encapsulates the slow time-varying behavior of the signal, while seasonal components capture periodicity. These techniques introduce interpretability in time series, which plays an important role in downstream tasks such as forecasting and anomaly detection. The classic approaches for decomposition are the widely used STL algorithm (Cleveland et al., 1990), and its variants (Wen et al., 2019; Bandara et al., 2022). Relevant to this work is the recent N-BEATS architecture (Oreshkin et al., 2020), a deep learning-based model for univariate time series forecasting that provides interpretability capabilities. The model explicitly encodes seasonal-trend decomposition into the network by defining separate trend and seasonal blocks, which fit a low degree polynomial and a Fourier series. While N-BEATS provides an interpretable decomposition, its applications do not cover multivariate time series and data synthesis. Desai et al. (2021) recently proposed TimeVAE, combining a VAE architecture with a trend-seasonality decomposition structure to allow for interpretable generation. However no results highlighting the advantages of this capability were demonstrated.

3 Formulation

In this Section, we describe the iSIREN network architecture for time series representation and interpretable decomposition, and the HyperTime and iHyperTime networks leveraged for prior learning and new data generation.

3.1 Time Series Representation

We consider a time series signal encoded by a discrete sequence of N observations $\mathbf{y} = (\mathbf{y}_1, ..., \mathbf{y}_N)$ where $\mathbf{y}_i \in \mathbb{R}^m$ is the m-dimensional observation at time t_i. This time series defines a dataset $\mathcal{D} = \{(t_i, \mathbf{y}_i)\}_{i=1}^N$ of time coordinates t_i associated with observations $\mathbf{y}_i$. We want to find a continuous mapping $f : \mathbb{R} \to \mathbb{R}^m, t \to f(t)$ that parameterizes the discrete time series, so that $f(t_i) = y_i$ for $i = 1...N$. The function f can be approximated by an implicit neural representation (INR) architecture conditioned on the training loss $\mathcal{L} = \sum_i \|y_i - \hat{f}(t_i)\|^2$. The network is composed of fully-connected layers with sine activations (SIREN) as defined by Sitzmann et al. (2020b):

$$\phi_j(\mathbf{x}_i) = \sin(\omega_0 \mathbf{W}_j \mathbf{x}_i + \mathbf{b}_j) \tag{1}$$

where $\phi_j(\cdot)$ corresponds to the j^{th} layer of the network. A general factor ω_0 multiplying the network weights determines the order of magnitude of the frequencies that will be used to encode the signal. Input and output of the INR are of dimensions 1 and m, corresponding to the time coordinate t and the prediction $\hat{f}(t)$. After training, the network encodes a continuous representation of the functional relationship $f(t)$ for a single time series.

3.1.1 Interpretable SIREN

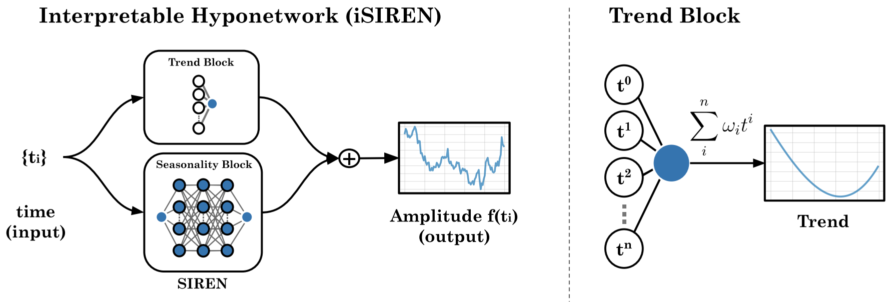

Figure 1: Interpretable SIREN (iSIREN) architecture comprised of two blocks. *Trend Block*:Single FC layer that outputs a polynomial fit of a fixed degree. *Seasonality Block*: SIREN network.

We propose an interpretable architecture to encode time series that reuses the INR with sine activation functions from the previous section. In particular, we assume that our INR follows a classic time series additive decomposition, i.e.,

$$f(t) = f_{\mathrm{tr}}(t) + f_{\mathrm{s}}(t), \tag{2}$$

where $f_{\mathrm{tr}}(t)$ represents the trend component and $f_{\mathrm{s}}(t)$ represents the seasonal component of $f(t)$, respectively. Note that this is a standard assumption for time series decomposition techniques, such as STL and others. We elaborate on the structure of $f_{\mathrm{tr}}(t)$ and $f_{\mathrm{s}}(t)$ in the following.

Trend block The trend component of a time series aims to model slow-varying (and occasionally monotonic) behavior. Following the work by Oreshkin et al. (2020) (N-BEATS), for the trend component of the interpretable architecture, we consider a polynomial regressor, i.e.,

$$f_{\mathrm{tr}}(t) = \sum_{i=0}^{p} \mathbf{w}_i^{(\mathrm{tr})} t^i, \tag{3}$$

where p denotes the degree of the polynomial, and $\mathbf{w}_i^{(\mathrm{tr})}$ denotes the weight vector associated with the ith degree. In practice, p is chosen to be small (e.g., $p = 2$) to capture low frequency behavior.

Seasonality block The seasonal component of the time series $f_{\mathrm{s}}(t)$ aims to capture the periodic behavior of the signal. In classical techniques, a pre-determined and fixed period (or set of periods) determines the resulting extracted seasonal components (e.g., STL supports single seasonal component, whereas MSTL supports multiple). In this work, we propose to model the seasonal component of the time series as a SIREN with J layers (see Section 3.1). Importantly, a single layer SIREN has been shown to be structurally similar to a Fourier mapped perception (FMP). An FMP $h : d_{\mathrm{in}} \to d_{\mathrm{out}}$ is a perceptron with identity activation and Fourier mapped input, i.e., for $\mathbf{x} \in \mathbb{R}^{d_{\mathrm{in}}}$ we have

$$h(\mathbf{x}) = \mathbf{W}^{\mathrm{FS}} \cdot \gamma(\mathbf{x}) + \mathbf{b}^{\mathrm{FS}}, \qquad \gamma(\mathbf{x}) = \begin{bmatrix} \cos(2\pi \mathbf{B} \cdot \mathbf{x}) \\ \sin(2\pi \mathbf{B} \cdot \mathbf{x}) \end{bmatrix}, \tag{4}$$

where $\mathbf{W}^{\mathrm{FS}} \in \mathbb{R}^{d_{\mathrm{out}} \times 2M}$ is a Fourier weight matrix, $\mathbf{b}^{\mathrm{FS}} \in \mathbb{R}^{d_{\mathrm{out}}}$ and $\gamma(\mathbf{x})$ is a Fourier mapping of the input $\mathbf{x}$, with $\mathbf{B} \in \mathbb{R}^{M \times d_{\mathrm{in}}}$ the Fourier mapping matrix of M frequencies. For a particular choice of $\mathbf{B}$ and $\mathbf{b}^{\mathrm{FS}} = \mathbf{0}$, an FMP is equivalent to a Fourier series representation and the Fourier mapping $\gamma(\mathbf{x})$ is equivalent to a single layer SIREN with fixed Fourier mapping matrix (Benbarka et al., 2022). A Fourier series is precisely what is used in the N-BEATS algorithm to model the seasonal component of the time series (Oreshkin et al., 2020). The benefit of using a SIREN is that the Fourier mapping becomes a trainable parameter – enabling the learning of the seasonal component of the time series in an *unsupervised* manner.

Training of iSIREN The training of iSIREN is performed in a supervised manner with an MSE reconstruction loss, as described for SIREN in Section 3.1. However, in order to stabilize the training, the process is performed in two stages: 1) we train the Trend Block for 100 epochs, computing the MSE loss between the ground truth time series $\mathbf{y}$ and the output of the block: $\mathcal{L}_1 = \sum_i \|y_i - \hat{f}_{\mathrm{tr}}(t)\|^2$. This leads to a smooth approximation of the time series, which we use as initial guess for the second stage. 2) We then train the Trend and Seasonality blocks together, computing the MSE reconstruction loss between the ground truth and the added output of both iSIREN blocks: $\mathcal{L}_2 = \sum_i \|y_i - \hat{f}(t_i)\|^2$.

3.2 Time Series Generation with HyperTime

In Figure 2-top, we display a diagram of the HyperTime architecture, which allows us to leverage INRs to learn priors over the space of time series. The Set Encoder (green network), composed of SIREN layers (Sitzmann et al., 2020b), takes as input a pair of values, corresponding to the time-coordinate t and the time series signal $f(t)$. Each pair of values is thus encoded into an embedding and evaluated by the HyperNet decoder (blue network), composed of fully-connected layers with ReLU activations (MLP). The output of the HyperNet is a one-dimensional vector that contains the network weights of an INR which encodes the time series data from the input. The INR architecture used within HyperTime is our interpretable SIREN (iSIREN), discussed in the previous section and illustrated in Figure 1. However, in Section 4.2 we will also consider the case of using SIREN as target INR. Following previous works (Sitzmann et al., 2020a), in the context of hypernetworks we refer to these predicted INRs as HypoNets in order to avoid ambiguities.

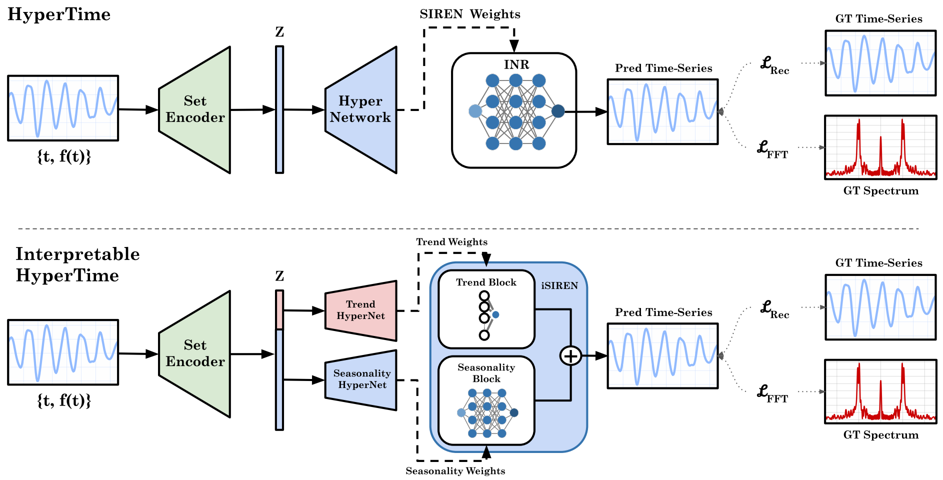

Figure 2: Diagram of HyperTime network architecture. Each pair of time-coordinate t and time series $f(t)$ is encoded as a 40-values embedding Z by the Set Encoder. The HyperNet decoder learns to predict HypoNet weights from the embeddings. During training, the output of the HyperNet is used to build a HypoNet and evaluate it on in the input time-coordinates. The loss is computed as a difference between $f(t)$ and the output of the HypoNet $\hat{f}(t)$.

During the training of HyperTime, we use the weights predicted by the HyperNet decoder to instantiate a HypoNet and evaluate it on the input time-coordinate t, to produce the predicted time series value $\hat{f}(t)$. The entire chain of operations is implemented within the same differentiable pipeline, and hence the training loss can be computed as the difference between the ground truth time series signal $f(t)$ and the value predicted by the HypoNet $\hat{f}(t)$.

The use of a Set Encoder in the architecture introduces permutation invariance in the computation. This enables the encoding of data with missing values or irregularly sampled, which are common occurrences in time series datasets. After training, the Set Encoder is able to generate latent embeddings Z to encode entire time series. In Section 4.2, we show that these embeddings can be interpolated to produce new samples from the distribution learned by the network, enabling the synthesis of new time series from known ones.

Training Loss The training of HyperTime is done by optimizing the following loss, which contains an MSE reconstruction term $\mathcal{L}_{\text{rec}}$ and two regularization terms $\mathcal{L}_{\text{weights}}$ and $\mathcal{L}_{\text{latent}}$, for the network weights and the latent embeddings, respectively:

$$\mathcal{L} = \underbrace{\frac{1}{N}\sum_{i=1}^{N}\left\|f(t_i) - \hat{f}(t_i)\right\|^2}_{\mathcal{L}_{\text{rec}}} + \lambda_1 \underbrace{\frac{1}{W}\sum_{j=1}^{W} w_j^2}_{\mathcal{L}_{\text{weights}}} + \lambda_2 \underbrace{\frac{1}{Z}\sum_{k=1}^{Z} z_k^2}_{\mathcal{L}_{\text{latent}}} + \lambda_3 \mathcal{L}_{\text{FFT}}. \tag{5}$$

Since we are working with time series, we want to ensure an accurate reconstruction not only of the signal but also of its spectral composition. Hence, we introduce an additional Fourier-based loss $\mathcal{L}_{\text{FFT}}$ that penalizes differences in the distribution of frequencies of the INR-encoded time series with respect to the ground truth data:

$$\mathcal{L}_{\text{FFT}} = \frac{1}{N}\sum_{i=1}^{N}\left\|\text{FFT}[f(t)]_i - \text{FFT}[\hat{f}(t)]_i\right\|. \tag{6}$$

In Section 4.2, we show that $\mathcal{L}_{\text{FFT}}$ is crucial for the accurate reconstruction of some datasets that show large variations of amplitudes in the frequency domain.

3.3 Interpretable HyperTime

In the previous section, we proposed a hypernetwork architecture (HyperTime) to learn a prior over a dataset of time series, encoding each sample as a small embedding Z. Although the HT architecture uses interpretable SIRENs as HypoNetworks, the decomposition between trend and seasonality signals is limited to the predicted INR, and is not explicitly reflected in the generated embeddings.

In Figure 2-bottom, we display our interpretable HyperTime (iHT) network, which builds over the previous HyperTime architecture to incorporate interpretability into the latent representation. Here the embedding Z is split in two parts Z_T and Z_S, corresponding to the encodings of the Trend and Seasonality signals. Each of these two embeddings is decoded by a different HyperNetwork (Trend HyperNet and Seasonality HyperNet) and affects the weights of a different block (Trend Block and Seasonality Block) within the predicted iSIREN. Only at the output of the iSIREN both signals are recomposed into a predicted time series, which is compared against the ground truth signal via the reconstruction and spectral losses ($\mathcal{L}_{Rec}$ and $\mathcal{L}_{FFT}$).

The training of iHyperTime is performed in two stages, in order to improve stability, as explained for iSIREN in Section 3.1.1. After training, the Set Encoder produces a decomposed encoding of time series into interpretable embeddings Z_T and Z_S. As with the HyperTime architecture, these embeddings can be interpolated to produce new unseen time series. However, as we will show in Section 4.2, we can now interpolate only one of the embeddings while leaving the other fixed. This way we can interpolate between time series with different trends while keeping the seasonality fixed and vice-versa allowing us to introduce fixed temporal structures to the data generation which can be used to inject domain expertise in cases where there is not sufficient data.

4 Experiments

4.1 Reconstruction

We start by analyzing the reconstruction performance of our model iSIREN over univariate and multivariate time series datasets from the UCR archive (Bagnall et al., 2017). We selected datasets with varying lengths and numbers of features, and sampled 100 time series from each of them, training a single INR for each time series. We compare against other INRs with different activations functions (Tanh, ReLU, Sine) and with ReLU positional encoding (P.E.) (Mildenhall et al., 2020) using INRs with equal size (3 hidden layer of 60 FC neurons). In addition, iSIREN presents 4 more trainable parameters per time series feature, due to the Trend block.

In Figure 3, we display two measures of reconstruction error averaged over 100 samples of a dataset (`FordA`). Figure 3-top displays the MSE training loss of each model in log space as a function of the training epoch. We observe that both models based on sine activations converge to similarly low values of error. We can also see that iSIREN's convergence is delayed during the first training iterations due to the sequential training of the Trend and Seasonality blocks, detailed in Section 3.1.1.

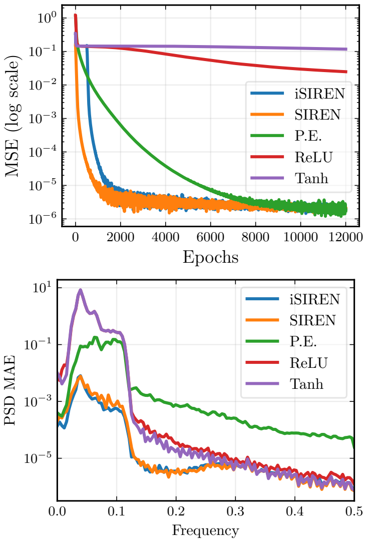

Figure 3: Comparison of iSIREN with other INR encodings. *Top:* MSE loss. *Bottom:* MAE of power spectral density.

In Figure 3-bottom, we focus on the accurate reconstruction of the GT spectral distribution. We illustrate the MAE of the power spectrum density (log) vs the frequency. Here we observe too that the lowest errors correspond to SIREN and iSIREN for all frequencies, with a slight advantage of our method for low frequencies. The reconstruction across all datasets has been summarized in Table 1, where we observe that iSIREN presents the best reconstruction performance, especially in terms of the spectral distribution. Moreover, for multivariate data iSIREN shows the lowest errors over all metrics and datasets, with a particularly large advantage in the case of `PhonemeSpectra`.

Finally in Figure 4, we illustrate the capacity of iSIREN to perform an interpretable decomposition of time series. In column (a) we show the signal reconstruction, and in columns (b) and (c) the corresponding outputs of the Trend and Seasonality blocks. As it would be expected, the Trend curve follows the overall shape of the signal, while the Seasonality prediction oscillates around zero. For a qualitative comparison, in columns (d) and (e) we see good agreement with an analogous decomposition performed by a traditional method (STL (Cleveland et al., 1990)). In contrast with iSIREN, STL requires prior knowledge of the frequency of the signal's seasonality.

Table 1: Comparison using MSE on time space and MAE in frequency space (FFT) of implicit networks using different activation functions and of iSIREN on univariate and multivariate datasets.

Dataset	iSIREN (Ours)		SIREN		P.E.		ReLU		Tanh	
	FFT	MSE	FFT	MSE	FFT	MSE	FFT	MSE	FFT	MSE
Univariate										
Crop	1.4e-3	5.6e-6	1.4e-3	1.6e-6	**6.8e-4**	**7.3e-7**	5.4e-1	2.1e-2	8.6e-1	6.0e-2
Energy	**4.1e-3**	**5.3e-6**	1.8e-2	1.2e-5	1.3e-1	7.7e-4	1.5e+0	4.9e-2	1.9e+0	8.3e-2
FordA	**1.7e-2**	**4.9e-6**	1.9e-2	6.2e-6	3.1e-1	2.1e-3	2.5e+0	1.3e-1	2.8e+0	1.4e-1
NonInv	**3.6e-2**	**1.2e-5**	4.0e-2	1.3e-5	1.1e-1	1.3e-4	1.0e+0	2.2e-2	1.3e+0	4.6e-2
Phalanges	**1.4e-3**	**2.1e-6**	3.8e-3	1.8e-6	7.6e-3	1.2e-5	2.4e-1	3.8e-3	7.5e-1	8.4e-2
Stock	**2.5e-3**	5.1e-6	4.4e-3	**1.4e-6**	4.3e-2	1.2e-4	6.2e-1	1.2e-2	8.9e-1	3.8e-2
Multivariate										
Cricket	**3.9e-1**	**4.1e-4**	4.5e-1	4.2e-4	1.7e+0	3.7e-3	3.5e+0	1.7e-2	3.9e+0	3.1e-2
MotorImagery	**5.1e+0**	**2.1e-3**	7.2e+0	6.2e-3	1.1e+1	2.4e-2	1.0e+1	2.6e-2	1.1e+1	3.0e-2
PhonemeSpectra	**2.9e-2**	**2.1e-6**	4.2e-1	2.7e-4	1.8e+0	5.9e-3	3.0e+0	1.5e-2	3.4e+0	2.0e-2

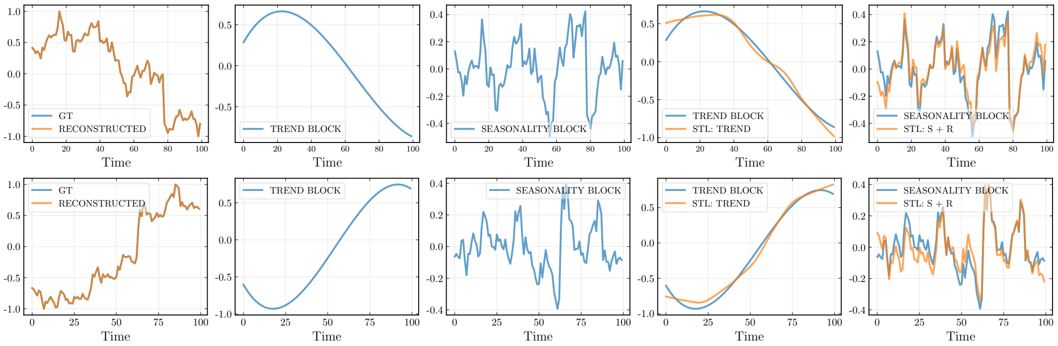

(a) Reconstruction (b) Trend (c) Seasonality (d) STL: trend (e) STL: seas

Figure 4: Interpretable decomposition of iSIREN on two time series from the `Stock` dataset. (a) Ground truth and iSIREN reconstruction. (b) Trend Block output. (c) Seasonality Block output. Columns (d) and (e) compare the output of iSIREN blocks with classic STL decomposition.

4.2 Time Series Generation

We leverage our proposed hypernetwork architectures for time series generation via the interpolation of latent representations. We follow the experimental set up proposed by Alaa et al. (2021) to evaluate our model on multiple datasets in terms of two metrics: 1) Predictive score (MAE), which measures how well the synthetic samples can be used to train a model and predict on real samples in a forecasting task. 2) F1-score, measuring the quality of the generated data via precision and recall metrics averaged over all time steps Sajjadi et al. (2018).

In Figure 5, we show qualitative evaluations of the generation performance for iHyperTime, and compare against multiple methods, including RealNVP Dinh et al. (2017) and current state-of-the-art for time series generation (TimeGAN Yoon et al. (2019b) and Fourier Flows Alaa et al. (2021)). We see a good agreement of iHyperTime for all datasets, while other methods fail to match the original data in some cases. Performance results using the Predictive score and F1-score metrics are summarized in Table 2. In addition to iHyperTime, we evaluate the following 3 other variations of the architecture:

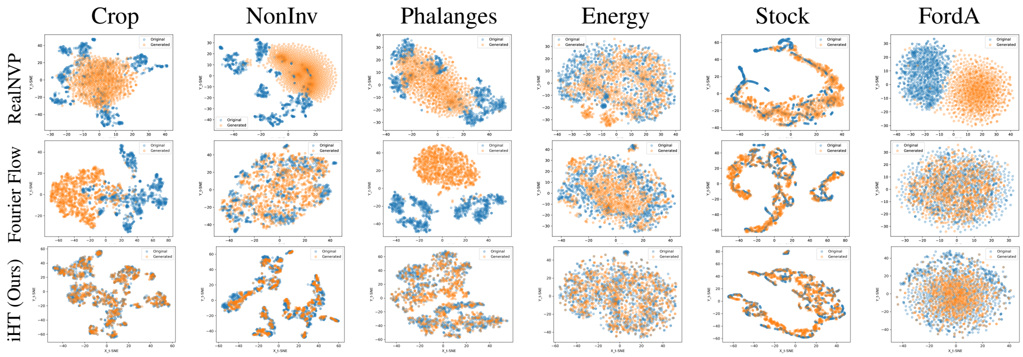

Figure 5: t-SNE visualization of real (blue) and synthetic (orange) data for all univariate datasets (in columns), using different time series generation methods (in rows).

HyperTime (no FFT): this architecture is directly based on one of the original hypernetwork architectures from SIREN (Sitzmann et al.).

HyperTime (w/FFT): same as previous, but including the FFT loss in the training.

HyperTime (iSIREN): same as previous, but using iSIREN as the predicted hyponetwork, thus generating time-series representations with built-in interpretable TS decomposition.

Table 2: Top: Performance scores for data generation using baselines and iHyperTime. Bottom: HyperTime ablations (in blue: values that improve over the baselines).

	Crop	**NonInv**	**Phalan.**	**Energy**	**Stock**	**FordA**
RealNVP						
MAE	0.170	0.038	0.073	0.036	0.019	0.115
F1 Score	0.981	0.986	0.976	0.964	0.977	**0.999**
TimeGAN						
MAE	0.048	–	0.108	0.056	0.173	–
F1 Score	0.831	–	0.960	0.479	0.938	–
Fourier Flows						
MAE	0.040	0.018	0.056	**0.030**	**0.010**	0.024
F1 Score	0.991	0.990	0.992	0.936	0.990	0.998
iHT (Ours)						
MAE	**0.039**	**0.004**	**0.024**	0.056	0.011	**0.009**
F1 Score	**0.999**	**0.997**	**0.997**	**0.997**	**0.995**	0.996
Ablations						
HT (no FFT)						
MAE	**0.040**	**0.005**	**0.023**	0.058	0.012	**0.170**
F1 Score	**0.999**	**0.996**	**0.996**	**0.998**	**0.995**	**0.084**
HT (w/ FFT)						
MAE	**0.040**	**0.005**	**0.023**	0.057	0.013	**0.007**
F1 Score	**0.999**	**0.997**	**0.999**	**0.997**	**0.994**	0.998
HT (iSiren)						
MAE	**0.039**	**0.004**	**0.024**	0.057	0.013	**0.008**
F1 Score	**0.999**	**0.997**	**0.999**	**0.997**	**0.995**	0.997

All hypernetwork architectures consistently generate high-quality synthetic time series, outperforming the baselines across most datasets and metrics. This indicates that the data generated by the HT and iHT architectures presents a high predictive utility for model training (Predictive score) and a large overlap with the distribution of the real data (F1 score).

An interesting failure case is presented with the generation of `FordA` samples by the **HT (no FFT)** model (in red). Here both evaluation metrics indicate a low performance. As shown in the supplemental material, the unusual diversity of spectral distributions present in the `FordA` dataset suggests that HT is unable to learn an effective reduced representation due to the complexity of the data. However, the issue is solved by the introduction of the spectral loss $\mathcal{L}_{FFT}$, as observed on the metrics for the **HT (w/FFT)** model. Moreover, the inclusion of this loss does not result in a loss of performance over other datasets.

Finally, in Figure 6 we illustrate the interpolation of interpretable embeddings from iHT. This model produces independent encodings Z_T and Z_S for the trend and seasonality signals, enabling additional control over the synthesis process by interpolating them separately. Figure 6a shows an interpolation of Z_S from source to target, leaving Z_T unchanged. By the end of the process, the interpolated time series has acquired the seasonality of the target signal, but maintains its original trend. Conversely, in Figure 6b we show an interpolation of the trend Z_T while fixing the seasonality Z_S. In both cases, we observe a smooth transition of the signal corresponding to the interpolated embedding, indicating a good generalization of the iHT architecture.

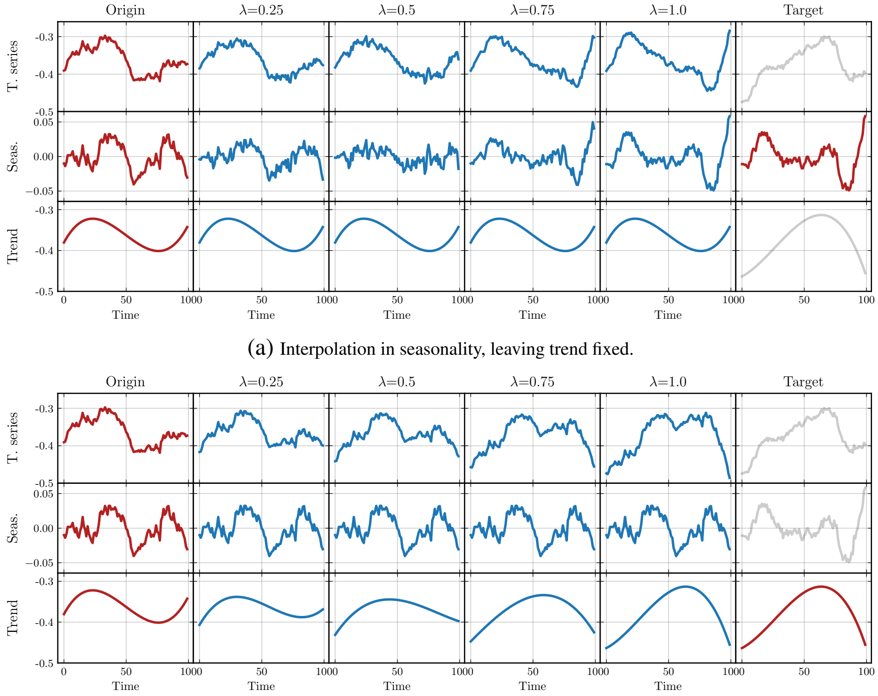

(a) Interpolation in seasonality, leaving trend fixed.

(b) Interpolation in trend, leaving seasonality fixed.

Figure 6: (a) Interpolation of seasonality, with fixed trend. (b) Interpolation in trend, with fixed seasonality. In red: original TS (1st column) and target seasonality/trend (last column).

5 Conclusions

In this work, we explored the use of INRs for the encoding and analysis of both univariate and multivariate time series data. We proposed a novel INR architecture (iSIREN) that enables learning an interpretable (seasonality-trend) continuous representation of time series data. We showed that our model outperforms other INRs in terms of the accurate reconstruction of the signal and its spectral distribution, with particular high performance for multivariate time series. Following this, we presented HyperTime, a hypernetwork architecture that leverages iSIRENs to learn a prior over a time series dataset. We demonstrated that by interpolating between embeddings learned by HT, we can generate new synthetic time series. To guide the training of HT, we introduced a Fourier-based loss that enforces the accurate reconstruction of the spectral distribution of the ground truth signals.

Finally we introduced iHyperTime, a hypernetwork model that incorporates interpretability into its latent representation of time series. We compared both HT and iHT against state-of-the-art methods for time series generation, showing improved results across most datasets and generative evaluation metrics. Furthermore, we showed that the disentangled seasonal-trend embeddings learned by iHT can be leveraged to introduce constraints into the generation, with potential applications for the incorporation of expert knowledge in the synthesis of new time series.

REFERENCES

Ahmed Alaa, Alex James Chan, and Mihaela van der Schaar. Generative time-series modeling with fourier flows. In *International Conference on Learning Representations*, 2021.

Ali Alqahtani, Mohammed Ali, Xianghua Xie, and Mark W. Jones. Deep time-series clustering: A review. *Electronics*, 10(23), 2021. ISSN 2079-9292. doi: 10.3390/electronics10233001. URL `https://www.mdpi.com/2079-9292/10/23/3001`.

Ivan Anokhin, Kirill V. Demochkin, Taras Khakhulin, Gleb Sterkin, Victor S. Lempitsky, and Denis Korzhenkov. Image generators with conditionally-independent pixel synthesis. *2021 IEEE/CVF Conference on Computer Vision and Pattern Recognition (CVPR)*, pp. 14273–14282, 2021.

Samuel A. Assefa, Danial Dervovic, Mahmoud Mahfouz, Robert E. Tillman, Prashant Reddy, and Manuela Veloso. Generating synthetic data in finance: Opportunities, challenges and pitfalls. In *Proceedings of the First ACM International Conference on AI in Finance*, ICAIF '20, New York, NY, USA, 2020. Association for Computing Machinery. ISBN 9781450375849. doi: 10.1145/3383455.3422554. URL `https://doi-org.manchester.idm.oclc.org/10.1145/3383455.3422554`.

A. Bagnall, J. Lines, A. Bostrom, J. Large, and E. Keogh. The great time series classification bake off: a review and experimental evaluation of recent algorithmic advances. *Data Mining and Knowledge Discovery*, 31:606–660, 2017.

Kasun Bandara, Rob J. Hyndman, and C. Bergmeir. Mstl: A seasonal-trend decomposition algorithm for time series with multiple seasonal patterns. *International Journal of Operational Research*, 2022.

Dimitrios Bellos, Mark Basham, Tony P. Pridmore, and Andrew P. French. A convolutional neural network for fast upsampling of undersampled tomograms in x-ray ct time-series using a representative highly sampled tomogram. *Journal of Synchrotron Radiation*, 26:839 – 853, 2019.

Nuri Benbarka, Timon Höfer, Hamd ul Moqeet Riaz, and Andreas Zell. Seeing implicit neural representations as fourier series. *2022 IEEE/CVF Winter Conference on Applications of Computer Vision (WACV)*, pp. 2283–2292, 2022.

Wei Cao, Dong Wang, Jian Li, Hao Zhou, Lei Li, and Yitan Li. Brits: Bidirectional recurrent imputation for time series. In S. Bengio, H. Wallach, H. Larochelle, K. Grauman, N. Cesa-Bianchi, and R. Garnett (eds.), *Advances in Neural Information Processing Systems*, volume 31. Curran Associates, Inc., 2018. URL `https://proceedings.neurips.cc/paper/2018/file/734e6bfcd358e25ac1db0a4241b95651-Paper.pdf`.

Eric Chan, Marco Monteiro, Petr Kellnhofer, Jiajun Wu, and Gordon Wetzstein. pi-gan: Periodic implicit generative adversarial networks for 3d-aware image synthesis. *2021 IEEE/CVF Conference on Computer Vision and Pattern Recognition (CVPR)*, pp. 5795–5805, 2021.

Yinbo Chen, Sifei Liu, and Xiaolong Wang. Learning continuous image representation with local implicit image function. In *Proceedings of the IEEE/CVF Conference on Computer Vision and Pattern Recognition*, pp. 8628–8638, 2021.

Kukjin Choi, Jihun Yi, Changhwa Park, and Sungroh Yoon. Deep learning for anomaly detection in time-series data: Review, analysis, and guidelines. *IEEE Access*, 9:120043–120065, 2021. doi: 10.1109/ACCESS.2021.3107975.

Robert B. Cleveland, William S. Cleveland, Jean E. McRae, and Irma Terpenning. Stl: A seasonal-trend decomposition procedure based on loess (with discussion). *Journal of Official Statistics*, 6: 3–73, 1990.

Abhyuday Desai, Cynthia Freeman, Zuhui Wang, and Ian Beaver. Timevae: A variational auto-encoder for multivariate time series generation. *arXiv preprint arXiv:2111.08095*, 2021.

Laurent Dinh, Jascha Sohl-Dickstein, and Samy Bengio. Density estimation using real NVP. In *International Conference on Learning Representations*, 2017. URL `https://openreview.net/forum?id=HkpbnH9lx`.

Chenguang Fang and Chen Wang. Time series data imputation: A survey on deep learning approaches. *ArXiv*, abs/2011.11347, 2020.

Elizabeth Fons, Paula Dawson, Xiao jun Zeng, John Keane, and Alexandros Iosifidis. Adaptive weighting scheme for automatic time-series data augmentation, 2021.

David Ha, Andrew M. Dai, and Quoc V. Le. Hypernetworks. In *5th International Conference on Learning Representations, ICLR 2017, Toulon, France, April 24-26, 2017, Conference Track Proceedings*. OpenReview.net, 2017. URL `https://openreview.net/forum?id=rkpACe1lx`.

Kyle Hundman, Valentino Constantinou, Christopher Laporte, Ian Colwell, and Tom Soderstrom. Detecting spacecraft anomalies using lstms and nonparametric dynamic thresholding. In *Proceedings of the 24th ACM SIGKDD International Conference on Knowledge Discovery &; Data Mining*, KDD '18, pp. 387–395, New York, NY, USA, 2018. Association for Computing Machinery. ISBN 9781450355520. doi: 10.1145/3219819.3219845. URL `https://doi-org.manchester.idm.oclc.org/10.1145/3219819.3219845`.

Hassan Ismail Fawaz, Benjamin Lucas, Germain Forestier, Charlotte Pelletier, Daniel F. Schmidt, Jonathan Weber, Geoffrey I. Webb, Lhassane Idoumghar, Pierre-Alain Muller, and François Petitjean. Inceptiontime: Finding alexnet for time series classification. *Data Mining and Knowledge Discovery*, 2020.

Kyeong-Joong Jeong and Yong-Min Shin. Time-series anomaly detection with implicit neural representation. *CoRR*, abs/2201.11950, 2022. URL `https://arxiv.org/abs/2201.11950`.

James Jordon, Jinsung Yoon, and Mihaela van der Schaar. Pate-gan: Generating synthetic data with differential privacy guarantees. In *ICLR*, 2019.

James Jordon, Daniel Jarrett, Evgeny Saveliev, Jinsung Yoon, Paul Elbers, Patrick Thoral, Ari Ercole, Cheng Zhang, Danielle Belgrave, and Mihaela van der Schaar. Hide-and-seek privacy challenge: Synthetic data generation vs. patient re-identification. In Hugo Jair Escalante and Katja Hofmann (eds.), *Proceedings of the NeurIPS 2020 Competition and Demonstration Track*, volume 133 of *Proceedings of Machine Learning Research*, pp. 206–215. PMLR, 06–12 Dec 2021. URL `https://proceedings.mlr.press/v133/jordon21a.html`.

Bryan Lim and Stefan Zohren. Time-series forecasting with deep learning: a survey. *Phylosophical Transactions of the Royal Society A*, 2021. doi: 10.1098/rsta.2020.0209.

Gidi Littwin and Lior Wolf. Deep meta functionals for shape representation. In *IEEE/CVF International Conference on Computer Vision (ICCV)*, pp. 1824–1833, 10 2019. doi: 10.1109/ICCV.2019.00191.

Yan Liu. Recurrent neural networks for multivariate time series with missing values. *Scientific Reports*, 8(1):6085, 2018. doi: 10.1038/s41598-018-24271-9. URL `https://doi.org/10.1038/s41598-018-24271-9`.

Yonghong Luo, Xiangrui Cai, Ying ZHANG, Jun Xu, and Yuan xiaojie. Multivariate time series imputation with generative adversarial networks. In S. Bengio, H. Wallach, H. Larochelle, K. Grauman, N. Cesa-Bianchi, and R. Garnett (eds.), *Advances in Neural Information Processing Systems*, volume 31. Curran Associates, Inc., 2018. URL `https://proceedings.neurips.cc/paper/2018/file/96b9bff013acedfb1d140579e2fbeb63-Paper.pdf`.

Qianli Ma, Jiawei Zheng, Sen Li, and Gary W Cottrell. Learning representations for time series clustering. In H. Wallach, H. Larochelle, A. Beygelzimer, F. d'Alché-Buc, E. Fox, and R. Garnett (eds.), *Advances in Neural Information Processing Systems*, volume 32. Curran Associates, Inc., 2019. URL `https://proceedings.neurips.cc/paper/2019/file/1359aa933b48b754a2f54adb688bfa77-Paper.pdf`.

Lars Mescheder, Michael Oechsle, Michael Niemeyer, Sebastian Nowozin, and Andreas Geiger. Occupancy networks: Learning 3d reconstruction in function space. In *Proceedings IEEE Conf. on Computer Vision and Pattern Recognition (CVPR)*, 2019.

Ben Mildenhall, Pratul P. Srinivasan, Matthew Tancik, Jonathan T. Barron, Ravi Ramamoorthi, and Ren Ng. Nerf: Representing scenes as neural radiance fields for view synthesis. In *ECCV*, 2020.

Cheolhwan Oh, Seungmin Han, and Jongpil Jeong. Time-series data augmentation based on interpolation. *Procedia Computer Science*, 175:64–71, 2020. ISSN 1877-0509. doi: https://doi.org/10.1016/j.procs.2020.07.012. URL `https://www.sciencedirect.com/science/article/pii/S1877050920316914`. The 17th International Conference on Mobile Systems and Pervasive Computing (MobiSPC),The 15th International Conference on Future Networks and Communications (FNC),The 10th International Conference on Sustainable Energy Information Technology.

Boris N. Oreshkin, Dmitri Carpov, Nicolas Chapados, and Yoshua Bengio. N-beats: Neural basis expansion analysis for interpretable time series forecasting. In *International Conference on Learning Representations*, 2020. URL `https://openreview.net/forum?id=r1ecqn4YwB`.

Mathias Perslev, Michael Jensen, Sune Darkner, Poul Jø rgen Jennum, and Christian Igel. U-time: A fully convolutional network for time series segmentation applied to sleep staging. In H. Wallach, H. Larochelle, A. Beygelzimer, F. d'Alché-Buc, E. Fox, and R. Garnett (eds.), *Advances in Neural Information Processing Systems*, volume 32. Curran Associates, Inc., 2019. URL `https://proceedings.neurips.cc/paper/2019/file/57bafb2c2dfeefba931bb03a835b1fa9-Paper.pdf`.

Tamar Rott Shaham, Michael Gharbi, Richard Zhang, Eli Shechtman, and Tomer Michaeli. Spatially-adaptive pixelwise networks for fast image translation. In *Computer Vision and Pattern Recognition (CVPR)*, 2021.

Mehdi S. M. Sajjadi, Olivier Bachem, Mario Lučić, Olivier Bousquet, and Sylvain Gelly. Assessing Generative Models via Precision and Recall. In *Advances in Neural Information Processing Systems (NeurIPS)*, 2018.

Vincent Sitzmann, Michael Zollhöfer, and Gordon Wetzstein. Scene representation networks: Continuous 3d-structure-aware neural scene representations. In *Advances in Neural Information Processing Systems*, 2019.

Vincent Sitzmann, Eric R. Chan, Richard Tucker, Noah Snavely, and Gordon Wetzstein. Metasdf: Meta-learning signed distance functions. In *Proc. NeurIPS*, 2020a.

Vincent Sitzmann, Julien N.P. Martel, Alexander W. Bergman, David B. Lindell, and Gordon Wetzstein. Implicit neural representations with periodic activation functions. In *Proc. NeurIPS*, 2020b.

Ivan Skorokhodov, Savva Ignatyev, and Mohamed Elhoseiny. Adversarial generation of continuous images. In *Proceedings of the IEEE/CVF Conference on Computer Vision and Pattern Recognition (CVPR)*, pp. 10753–10764, June 2021.

Alejandro Sztrajman, Gilles Rainer, Tobias Ritschel, and Tim Weyrich. Neural brdf representation and importance sampling. *Computer Graphics Forum*, 40(6):332–346, 2021. doi: https://doi.org/10.1111/cgf.14335. URL `https://onlinelibrary.wiley.com/doi/abs/10.1111/cgf.14335`.

Matthew Tancik, Pratul P. Srinivasan, Ben Mildenhall, Sara Fridovich-Keil, Nithin Raghavan, Utkarsh Singhal, Ravi Ramamoorthi, Jonathan T. Barron, and Ren Ng. Fourier features let networks learn high frequency functions in low dimensional domains. *NeurIPS*, 2020.

José F. Torres, Dalil Hadjout, Abderrazak Sebaa, Francisco Martínez-Álvarez, and Alicia Troncoso Lora. Deep learning for time series forecasting: A survey. *Big data*, 2021.

Svitlana Vyetrenko and Shaojie Xu. Risk-sensitive compact decision trees for autonomous execution in presence of simulated market response, 2019. URL `https://arxiv.org/abs/1906.02312`.

Qingsong Wen, Jingkun Gao, Xiaomin Song, Liang Sun, Huan Xu, and Shenghuo Zhu. Robuststl: A robust seasonal-trend decomposition algorithm for long time series. *Proceedings of the AAAI Conference on Artificial Intelligence*, 33(01):5409–5416, Jul. 2019.

Magnus Wiese, Robert Knobloch, Ralf Korn, and Peter Kretschmer. Quant gans: deep generation of financial time series. *Quantitative Finance*, pp. 1–22, Apr 2020. ISSN 1469-7696. doi: 10.1080/14697688.2020.1730426. URL http://dx.doi.org/10.1080/14697688.2020.1730426.

Gerald Woo, Chenghao Liu, Doyen Sahoo, Akshat Kumar, and Steven C. H. Hoi. Deeptime: Deep time-index meta-learning for non-stationary time-series forecasting. 2022. URL https://arxiv.org/abs/2207.06046.

Haowen Xu, Wenxiao Chen, Nengwen Zhao, Zeyan Li, Jiahao Bu, Zhihan Li, Ying Liu, Youjian Zhao, Dan Pei, Yang Feng, Jie Chen, Zhaogang Wang, and Honglin Qiao. Unsupervised anomaly detection via variational auto-encoder for seasonal kpis in web applications. In *Proceedings of the 2018 World Wide Web Conference*, WWW '18, pp. 187–196, 2018. ISBN 9781450356398. doi: 10.1145/3178876.3185996. URL https://doi-org.manchester.idm.oclc.org/10.1145/3178876.3185996.

Jinsung Yoon, Daniel Jarrett, and Mihaela van der Schaar. Time-series generative adversarial networks. In *NeurIPS*, 2019a.

Jinsung Yoon, Daniel Jarrett, and Mihaela van der Schaar. Time-series generative adversarial networks. In *NeurIPS*, 2019b.

Li Zeng, Baifan Zhou, Mohammad Al-Rifai, and Evgeny Kharlamov. Segtime: Precise time series segmentation without sliding window, 2022. URL https://openreview.net/forum?id=FqMXxvHquTA.